Chemical Engineering Journal 154 (2009) 219–230

Contents lists available at ScienceDirect

Chemical Engineering Journal

journal homepage: www.elsevier.com/locate/cej

Modelling of diesel filters for particulates removal

M. Schejbal[a], M. Marek[a,*], M. Kubíček[b], P. Kočí[a]

[a] Department of Chemical Engineering, Institute of Chemical Technology Prague, Technická 5, CZ-166 28 Prague, Czech Republic
[b] Department of Mathematics, Institute of Chemical Technology Prague, Technická 5, CZ-166 28 Prague, Czech Republic

ARTICLE INFO

Article history:
Received 25 November 2008
Received in revised form 3 April 2009
Accepted 23 April 2009

Keywords:
Diesel filter
Particulates removal
Soot oxidation

ABSTRACT

Diesel particulate filter (DPF) is regarded as the most useful technology to reduce particulate matter from exhaust gas of a diesel engine, with filtration efficiencies in excess of 90%. Exhaust gas entering the channel is forced to flow through the ceramic porous walls into the adjoining cells and thus leaving the particulates behind. The collected particulate matter inside the trap has to be periodically oxidized to regenerate the DPF. We have developed a transient spatially 2D model of the filter, soot deposition and its regeneration. The momentum, mass and enthalpy balances of the gas and the solid phase were employed in the model including the description of heat conduction, diffusion in the solid phase and complex soot combustion kinetics. Detailed kinetics of soot combustion is considered: combustion by O_2—both the thermal initiated one and the catalyzed one and the oxidation by NO_2. The results of simulations include the prediction of development of concentrations, temperature, pressure, flow pattern and soot layer thickness along the filter. Effect of NO_2-assisted soot oxidation coupled with catalytic NO/NO_2 transformation is examined. The filtration model includes cake and deep-bed filtration and it is used to predict porosity, permeability, filtration efficiency of the soot layer and the wall. Optimized numerical methods and software for the solution of the above mentioned models are described and results for various operation conditions are presented and discussed.

1. Introduction

Over half of the new cars sold in Europe are powered by diesel engines, because diesel engines are much more efficient than gasoline ones of the same power (common efficiency of gasoline engines is 26–30% and the efficiency of diesel engines in modern cars is approximately 45% [1]). This results in lower fuel consumption. However, diesel engine produces particles of carbonaceous soot (PM), which also consists of unburned organic compounds and other solid and liquid material. Particles are formed in local low temperature regimes (outside of big fuel droplets and on the walls) in diesel engine cylinders when fuel is not fully atomized. Widely used technology for diesel soot particle removal is diesel particulate filter (DPF). It is a flow-through monolithic device, similar to catalytic converter, which forces exhaust gas to flow through porous walls to clean solid particles (Fig. 1). DPF systems are designed with several requirements: effective PM filtration, minimal pressure drop, high durability, low service requirements and low cost. European Union emission regulations for new light vehicles (EURO 5,6) restricts PM to 5 mg/km. This limit must be met with low purchase and maintenance cost. Maintenance cost means predominantly cost of DPF passive or active regeneration. Passive DPF systems can be equipped by catalytic coating (CDPF) which lowers PM burning temperature or can use catalysts as fuel additives. Active DPFs are designed for one or combination of different regeneration method—filters regenerated by fuel combustion (post-injection), electrically or microwave regenerated filters. Costs with fixed operational properties could be optimized and effective technique to find Pareto multi-objective optimality is the subject of mathematical modelling of the DPF, considering catalyst and fuel price and many other factors. We have developed a versatile mathematical model of single pair of DPF channels (inlet and outlet) assuming that there are ash layer and washcoat catalyst coating in the inlet channel. Program code is written in Fortran and optimized for fast computing and kinetic parameters evaluation from experimental data. The used finite volume numerical method is suitable for description of processes taking place on several layers with different kinetics in perpendicular direction to wall and also along the zoned coating of the washcoat [2]. The purpose of this work was to develop comprehensive mathematical model of nonstationary behaviour of the DPF including detailed description of soot oxidation kinetics by NO_2. As critical model parameters have to be evaluated from experimental data, effective numerical methods were used in the developed software. Examples of model validation are given. Acceptable computational times and flexible structure of the model enable its use in DPF design.

* Corresponding author. Tel.: +420 22044 3104; fax: +420 22044 4320.
E-mail address: milos.marek@vscht.cz (M. Marek).
URL: http://www.vscht.cz/monolith (M. Schejbal).

1385-8947/$ – see front matter © 2009 Elsevier B.V. All rights reserved.
doi:10.1016/j.cej.2009.04.056

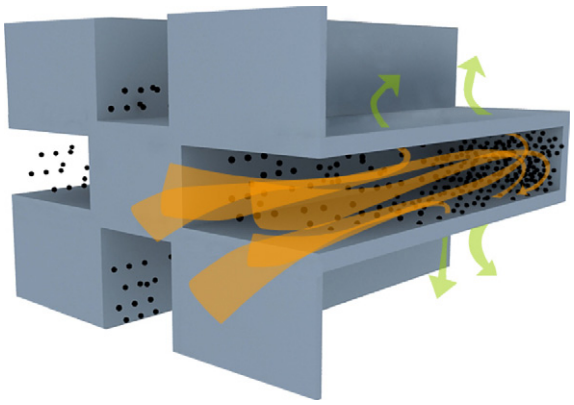

Fig. 1. Sketch of the flow trough the channel wall.

2. Mathematical model of single pair of channels

The model has been developed on a similar basis as the single-channel models [3–5] derived from the classical Bissett model [6]. However, modifications consisting of the use of three different layers—ash, washcoat and soot, other choice of boundary conditions and different numerical solution method were used. The model includes mass, momentum and enthalpy balances. The main assumptions are:

- The filter is in a quasistationary state, gas residence time is very small.
- Radial changes of temperature, concentration and gas velocity in the gas phase are negligible and also axial dispersion is neglected.
- Temperature gradients in the solid phase in the direction of x-axis (cf. Fig. 2) can be neglected under certain conditions. Validity of this assumption is discussed in [7].
- All pairs of channels are the same. The model assumes uniform flow distribution at the filter front face and an adiabatic operation.

Component balances and soot combustion model are solved within the soot cake, ash layer, washcoat coating and porous wall. The density of the gas is approximated by the density of ideal gas.

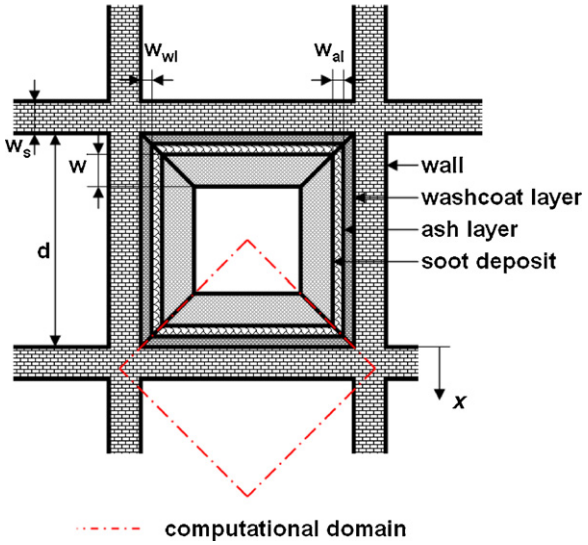

Fig. 2. Front scheme of the inlet channel.

2.1. Temperature of solid phase

Under the above mentioned assumptions model equation for temperature of the wall and of the soot layer is

$$\frac{\partial T_S}{\partial t} = \frac{\lambda_S}{\rho_S C_{p,S}} \frac{\partial^2 T_S}{\partial z^2} + \frac{S}{A_S \rho_S C_{p,S}} \tag{1}$$

The heat source term S includes the contributions of heat transfer, convection of heat between solid phase and gas phase and heat of reactions

$$S = H_{transf} + H_{conv} + H_{react} \tag{2}$$

The individual terms in H_{transf} are heat transfer from the flowing gas in the inlet channel to the solid and from the solid to the outlet channel:

$$H_{transf} = 4d_1 k_{h,1}(T_1 - T_S) + 4d_2 k_{h,2}(T_2 - T_S) \tag{3}$$

For the computation of the heat (and mass) transfer coefficients for each channel we have used the procedure described by Ramanathan et al. [8]. For the convection term H_{conv} we have:

$$H_{conv} = 4d\phi_S C_{p,g} T_1 - 4d\phi_S C_{p,g} T_S \tag{4}$$

The heat evolved by the reactions is integrally averaged in the solid phase area according to:

$$H_{react} = \int_{-w-w_{al}-w_{wl}}^{w_s} A_x \sum_k \mathcal{R}_k \Delta H_k^r \, dx \tag{5}$$

A_x is the perimeter of computed discretization volume. Parabolic partial differential equation (1) is then solved with boundary and initial conditions:

$$\left.\frac{\partial T_S}{\partial z}\right|_{z=0,L} = 0 \tag{6}$$

$$T_S\big|_{t=0} = T_S^{ini} \tag{7}$$

The balanced elementary volume for heat balance dV_S is defined as $A_S dz$, where

$$A_S = \frac{(d + 2w_s)^2 - (d - 2(w + w_{al} + w_{wl}))^2 - 2w_s^2}{4} \tag{8}$$

2.2. Mass balances of flowing gas

Soot cake has nonzero volume and thus (cf. Fig. 3)

$$d_1(z) = d - 2(w(z) + w_{al} + w_{wl}) \tag{9}$$

$$d_2 = d \tag{10}$$

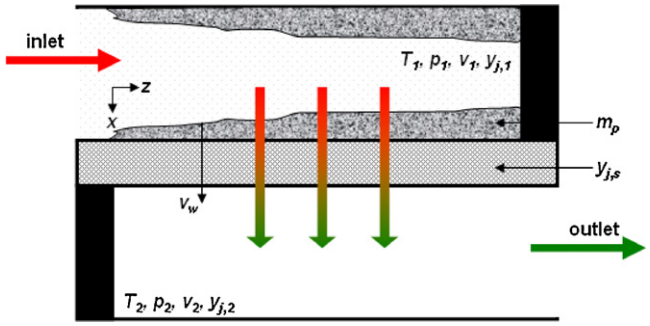

Fig. 3. Side scheme of the DPF.

holds for inlet and outlet channel and the flow field in the inlet channel is governed by equation:

$$\frac{\partial(d_1^2\phi_1)}{\partial z} = -4d\phi_S \tag{11}$$

and similar equation for the outlet channel:

$$d_2^2\frac{\partial\phi_2}{\partial z} = 4d\phi_S \tag{12}$$

The wall-through mass flux ϕ_S is related to reference area dh_z, where d is the hydraulic diameter of the outlet channel and thus it is considered $\phi_S = \dot{m}/(dh_z)$. Mass balances are solved with the following boundary condition—inlet gas flux

$$\phi_1|_{z=0} = \frac{\dot{m}_{in}}{OFA} = \frac{\dot{m}_{in}}{N_{chan}d_1^2|_{z=0}} \tag{13}$$

2.3. Momentum balance of the flowing gas

Balances of momentum in the direction of the z axis for both channels are given by:

$$\frac{\partial(d_1^2 p_1)}{\partial z} + \frac{\partial}{\partial z}(d_1^2\phi_1^2/\rho_1) = -\alpha\mu\phi_1/\rho_1 \tag{14}$$

$$\frac{\partial p_2}{\partial z} + \frac{\partial}{\partial z}(\phi_2^2/\rho_2) = -\frac{\alpha\mu\phi_2/\rho_2}{d_2^2} \tag{15}$$

Solution of these equations gives pressures in the inlet and outlet channels. The terms $(\partial/\partial z)(d_i^2\phi_i^2/\rho_i)$, $i = 1, 2$ could be neglected, because the gas flow is laminar in both channels. α is a constant in channel pressure drop correlation and is equal to 28.454 cf., e.g., [9]. It is assumed that outlet pressure is known and the boundary condition is $p_2|_{z=L} = p_{atm} + \Delta p_{expansion} + \Delta p_{outlet\ cone}$.

2.4. Pressure drop

The overall pressure drop of the filter consists of several contributions:

$$\begin{aligned}\Delta p_{DPF} = {} & \Delta p_{inlet\ cone} + \Delta p_{contraction} + \Delta p_{inlet\ channel} \\ & + \Delta p_{soot+ash+washcoat} + \Delta p_{wall} + \Delta p_{outlet\ channel} \\ & + \Delta p_{expansion} + \Delta p_{outlet\ cone}\end{aligned} \tag{16}$$

Here the pressure difference across the porous wall can be described by Darcy's law (characterizes viscous effects) with Forchheimer extension (characterizes inertia effects)

$$\Delta p_{wall} = \frac{\mu\phi_S/\rho_S}{k_{wall}}w_s + \frac{\beta_{wall}w_s}{\rho_S}\phi_S^2 \tag{17}$$

and for soot, washcoat and ash layers we have used the same equation written for trapezoidal shape of the layers:

$$\Delta p_i = \frac{1}{2}\frac{\mu\phi_S d}{\rho_S k_i}\ln\left(\frac{d_i}{d_i - 2w_i}\right) + \frac{\beta_i}{\rho_S}\phi_S^2 d^2\frac{w_i}{d_i(d_i - 2w_i)} \tag{18}$$

This equation represents pressure drop of the layer i with the thickness w_i and the basis width d_i. Two parameters (permeability and Forchheimer factor) must be evaluated from laboratory measurements. Comparison of our simulations with measured data showed that Darcy's law is quite sufficient and Forchheimer second-order term may be neglected for low wall-flow velocities [10]. Sudden pressure losses due to contraction and expansion at the inlet and at the outlet of the chessboard patterned face of the filter can be calculated from the equation

$$\Delta p_{contraction} = \frac{\zeta_{in}\dot{m}^2}{2d^4\rho_{in}} \tag{19}$$

$$\Delta p_{expansion} = \frac{\zeta_{out}\dot{m}^2}{2d^4\rho_{out}} \tag{20}$$

ζ_{in} and ζ_{out} are functions of the percentage of the open frontal area. The pressure drop of the inlet cone and the outlet cone of the DPF housing is included in Eq. (16). The pressure drop of the inlet and the outlet cone strongly depends on the cone geometry and will normally be calculated using CFD in the design phase. An approximate calculation of the cone pressure drop can be done using the following equation [11]:

$$\Delta p_{inlet\ cone} = \zeta_{inlet\ cone}\left(1 - \frac{A_{inlet\ tube}}{A_{DPF}}\right)\frac{\rho}{2}v_{inlet\ tube}^2 \tag{21}$$

The pressure drop of the outlet cone can be determined in the same way:

$$\Delta p_{outlet\ cone} = \zeta_{outlet\ cone}\frac{\rho}{2}v_{outlet\ tube}^2 \tag{22}$$

The resistance factors $\zeta_{inlet\ cone}$ and $\zeta_{outlet\ cone}$ can be determined according to [12] as a function of the diffuser angle and as a function of the expansion ratio.

2.5. Enthalpy balance of the flowing gas

Enthalpy balance for the inlet channel is

$$\frac{\partial(d_1^2 C_{p,g}\phi_1 T_1)}{\partial z} = 4d_1 k_{h,1}(T_S - T_1) - 4d\phi_S C_{p,g}T_1 \tag{23}$$

and for the outlet channel analogously

$$\frac{\partial(d_2^2 C_{p,g}\phi_2 T_2)}{\partial z} = 4d_2 k_{h,2}(T_S - T_2) + 4d\phi_S C_{p,g}T_S \tag{24}$$

Solution of the enthalpy balances of gas yields temperature profiles along the filter in the inlet and outlet channels. Equations describing temperature in both channels are solved with the boundary condition—inlet temperature $T_1|_{z=0} = T_{in}$.

2.6. Component balances in the flowing gas

Component mass balances in the flowing gas in the inlet and the outlet channel are:

$$\frac{\partial(d_1^2\phi_1 y_1^j)}{\partial z} = -4d\phi_S y_1^j + 4d_1 k_{c,1}^j(y_{S^1}^j - y_1^j), \quad j = 1, \ldots, J \tag{25}$$

$$\frac{\partial(d_2^2\phi_2 y_2^j)}{\partial z} = 4d\phi_S y_{S^2}^j - 4d_2 k_{c,2}^j(y_2^j - y_{S^2}^j), \quad j = 1, \ldots, J \tag{26}$$

The component balances satisfy boundary conditions:

$$y_1^j|_{z=0} = y_{in}^j, \quad j = 1, \ldots, J \tag{27}$$

2.7. Component balance in the radial direction

Mass balances of gaseous components in the soot cake and in the wall are given by the following reaction–diffusion–convection equations (quasistationary behaviour is assumed):

$$\phi_S\frac{\partial y_S^j}{\partial x} - D_j\rho_S\left(\frac{\partial^2 y_S^j}{\partial x^2}\right) = M^j\sum_k \mathcal{R}_k, \quad j = 1, \ldots, J \tag{28}$$

Boundary conditions for Eq. (28) are derived from (25) and (26) and from the balances at the boundary S^1 between the solid phase (soot cake or wall) and gas in the inlet channel. Differential replacement with respect to used finite volume method is

$$-P(x)h_x M^j \sum_k \mathcal{R}_k - d\phi_S y^j_{S^1} + d_1 D_j \rho_S \frac{y^j_{S^1} - y^j_{S^2}}{h_x}$$
$$= -d\phi_S y^j_1 + d_1 k^j_{c,1}(y^j_{S^1} - y^j_1), \quad j = 1, \ldots, J \tag{29}$$

The boundary conditions for boundary S^2 between solid phase (wall) and gas in the outlet channel are similarly

$$-P(x)h_x M^j \sum_k \mathcal{R}_k - d_2 D_j \rho_S \frac{y^j_{S^{N_x-1}} - y^j_{S^{N_x}}}{h_x}$$
$$= -d_2 k^j_{c,2}(y^j_2 - y^j_{N_x}), \quad j = 1, \ldots, J \tag{30}$$

Component balance in the x-direction is discretized into finite volumes with the base area $A(x)$ and the height h_x. The area $A(x)$ can be decomposed to $A(x) = P(x)\partial z$, where the perimeter $P(x)$ in the x-direction is equal to:

$$P(x) = \begin{cases} (d + 2x), & x < 0 \text{(soot cake,ash or washcoat layer)} \\ d, & x \geq 0 \text{(wall)} \end{cases} \tag{31}$$

Influence of diffusion of reaction components has been discussed, e.g., in [4,13]. Authors have concluded that the diffusion can be important in some simulation cases, e.g., diffusion in porous wall can affect reaction rates during uncontrolled regeneration. Computation of effective diffusivity coefficients in the soot cake and in the wall is based on the effective diffusion model. We consider molecular and Knudsen diffusion mechanisms in the bulk gas and in the pores. Suitable relation (Bosanquet formula) for the estimation of additive–resistance diffusivity coefficient is

$$\frac{1}{D^{\text{eff}}_j} = \frac{\tau}{\varepsilon}\left(\frac{1}{D^{\text{vol}}_j} + \frac{1}{D^{\text{Knudsen}}_j}\right) \tag{32}$$

where the Knudsen diffusion coefficients D^{Knudsen}_j for each gas component are computed as

$$D^{\text{Knudsen}}_j = \frac{d_p}{3}\sqrt{\frac{8RT}{\pi M^j}} \tag{33}$$

and the volume diffusion coefficients D^{vol}_j are computed by Fuller equation [14]. Diffusion flux across the layer boundary is given by the harmonic average of diffusivities of both phases.

2.8. Conservation of soot mass in the cake and in the wall

Soot mass time variation in the soot layer and in the wall is defined as

$$\frac{\partial m_p}{\partial t} = M^p V_{\text{FVM}} \sum_k \mathcal{R}_k - E_{DP} \tag{34}$$

Soot is consumed by oxidation reactions, but additional soot mass E_{DP} is continuously accumulated from the exhaust gas. The term E_{DP} is determined by deep-filtration model described in the next section. Soot particles in the soot layer are transported down from one layer to another. Soot particles density in the soot layer varies between approx. 40 and 100 kg/m^3 and could be a function of distance from the wall surface after compression by high air flow [15].

2.9. Deep-filtration model

Deep-filtration model using the approach described also in [9,16–18] is solved simultaneously, with the main single-channel model. It is based on the application of the 'unit collector' model on discretized volumes in all layers where soot particles are trapped. The overall collection efficiency of layer i can be expressed as

$$\eta_f = 1 - \exp\left(-\int_0^{w_i} \frac{4\eta\alpha_f}{\pi(1-\alpha_f)d_c}\,\mathrm{d}x\right) \tag{35}$$

where η is the combined single-sphere efficiency of individual deposition mechanisms, namely, the Brownian diffusion and the interception:

$$\eta = 1 - (1 - \eta_D)(1 - \eta_R) \tag{36}$$

The collection efficiency of single sphere due to Brownian diffusion may be estimated as

$$\eta_D = 3\left(\frac{1-\alpha_f}{\text{Ku}(\varepsilon)}\right)^{1/3} \text{Pe}^{-2/3} \tag{37}$$

Péclet number is defined as $\text{Pe} = (Ud_c/D) = (12\pi\phi_S d\mu d_p d_c/\varepsilon\rho_S P(x)\text{SCF}k_b T)$. The collection efficiency by the interception is given by:

$$\eta_R = 1.5\frac{1-\alpha_f}{\text{Ku}(\varepsilon)}\frac{(d_p/d_c)^2}{(1+(d_p/d_c))^{(3-2\varepsilon)/3\varepsilon}} \tag{38}$$

We have assumed that the Brownian diffusion and the interception are independent of each other. Their dependence on the particle diameter is opposite—as d_p increases Brownian diffusion efficiency decreases due to the decrease of diffusion coefficient and the interception efficiency increases with the increasing d_p due to increasing interception parameter (d_p/d_c). Other well-known mechanism – the inertial impaction – is significant for higher velocities and for large particles and it could be neglected for typical DPF applications ($d_p < 1\,\mu$m). Total soot mass of unit collector in every slab volume is calculated by the local collection efficiency η_f and with entering particle distribution. Deposited soot mass modifies local unit collector diameter, porosity and permeability in (x, y)-position of the ash layer, the washcoat layer and the wall:

$$d_c(x,z) = 2\left[\frac{3m_p(x,z)}{4\pi\rho_p N_{\text{UN}}} + \left(\frac{d_{c,\text{ini}}}{3}\right)^2\right]^{1/3} \tag{39}$$

$$\varepsilon(x,z) = 1 - \left(\frac{d_c}{d_{c,\text{ini}}}\right)^3 \alpha_{\text{ini}} \tag{40}$$

$$k(x,z) = k_{\text{ini}}\left(\frac{d_c}{d_{c,\text{ini}}}\right)^2 \frac{\text{Ku}(\varepsilon)}{\text{Ku}(\varepsilon_{\text{ini}})}\frac{\alpha_{\text{ini}}}{\alpha} \tag{41}$$

The initiation of cake filtration depends on filtration efficiency of the first wall slab, which determines the fraction of mass deposited as particulate layer and the mass deposited inside the wall—higher pore bridging percolation factor allows more particles to be deposited inside the wall. All soot loading computations are calculated for number particle distribution under assumption that all particles have the same density and spherical shape. Computation of the outlet particle distribution is useful for comparison with the proposed EU emission number limit of Euro 5/6 standard—5×10^{11} particles per km [1].

3. Solution procedure

We have developed original software for the numerical solution of the above described set of channel scale model equations. The software is written in Fortran 77 and its main advantage is short computation time following from extensive optimization of proper numerical methods and problem decomposition. The model software can thus be used also as a subroutine in kinetic data evaluation

from soot combustion experiments. Numerical solution of PDE system is based on the discretization of x, z and t coordinates by the finite volume method (FVM) and the resulting system of nonlinear equations has been solved by the modified Newton method. System of linear equations with Jacobi matrix is solved by special solver for sparse matrix with diagonal band. We have used second-order accurate interpolation for representing interface values. Parabolic equation for computing temperature profile of the solid has been discretized into volumes by the Crank–Nicolson scheme. Time integration of differential equations gives solution of local and transient variables in each axial and radial node. Mass flow, temperature, pressure and species concentrations profiles in both channels are obtained. The deep-filtration model of layers is solved simultaneously with the channel model and the initial conditions for the regeneration simulations are obtained by the use of the solely deep-filtration model. Proper strategy of alternating between the soot loading and the channel simulation can be chosen. This can reduce the computation time: the deep-filtration model described by algebraic equations can be solved much faster than the complete channel model described by PDE's. Real timescale of processes in the DPF also vary—the filter loading is of the order of hours, active regeneration is of the order of minutes, passive regeneration is a continual process. Proper combination of the models used can reduce computation time, e.g., the use of only deep-filtration model for long filter loading and the switching to complete model for DPF active regeneration.

Time step for the integration of the DPF model is adaptively controlled in dependence on temperature, concentration and soot mass changes in chosen finite volumes. Overall time for the integration of 1 s real time with sufficient accuracy (typically $h_z = L/25$, $h_{x,\mathrm{wall}} = w_s/25$ in the simulation of uncoated 300 cpsi SiC filter with $D_{\mathrm{DPF}} = 144\,\mathrm{mm}$, $L = 150\,\mathrm{mm}$ and $w_s = 356\,\mu\mathrm{m}$) is approximately 0.2 s of CPU time (3.5 GHz PC).

4. Reactions and kinetics

4.1. Oxidation of particulate matter

Diesel particulate matter are small graphitic carbon particles on which aromatic, paraffinic and other oxygenated organic components are adsorbed. Composition of particulates in diesel exhaust depends on several characteristics—engine load and type, speed, used fuel and lubricants and many other factors. DPM is thus divided into three fractions: solid fraction (elemental carbon-soot, ash), soluble organic fraction (SOF) derived from lubricants and fuel, and sulfate particulates [1]. C/H ratio is an indication of the adsorbed hydrocarbons content. Estimation of particulates mass could be obtained by thermogravimetry using a procedure based on different treatments of the real particulate under inert and oxidative carrier gas [19]. The weight fraction due to hydrocarbons is close to 50%. Oxidation of the DPM by O_2 could be described by the summary reaction:

$$\mathrm{C}_x\mathrm{H}_y + \left[x\left(1 - \frac{f_{\mathrm{CO}}}{2}\right) + \frac{y}{4}\right]\mathrm{O}_2 \rightarrow x f_{\mathrm{CO}}\mathrm{CO} + x(1 - f_{\mathrm{CO}})\mathrm{CO}_2 + \frac{y}{2}\mathrm{H}_2\mathrm{O} \tag{42}$$

However, in this work it is assumed that DPM contains only elementary or organic carbon of the SOF part and thus the following reactions are considered to take place in the soot cake, ash, washcoat layer and in the wall:

$$\mathrm{C} + \left(1 - \frac{f_{\mathrm{CO}}}{2}\right)\mathrm{O}_2 \rightarrow f_{\mathrm{CO}}\mathrm{CO} + (1 - f_{\mathrm{CO}})\mathrm{CO}_2 \tag{43}$$

Soot combustion temperature without catalyst is close to 600 °C or approximately 450 °C in the presence of Pt-doped catalyst (depends on the weight fraction of Pt in the carrier—CeO_2 or CeO_2La [20]). Local reaction rate is given by the relation

$$\mathcal{R}_{43} = k_{43}\left(\frac{m_p}{\rho_p V_{\mathrm{FVM}}\varepsilon_i^0}\right)^{n_\xi} c_{\mathrm{O}_2}^{0.8} \tag{44}$$

where n_ξ is the reaction order in carbon. We have used the value 0.73 [21] for real diesel soot, which is close to the order 0.67 applicable for the shrinking-core model. We have used for the reaction (43) special form of a temperature dependence of reaction kinetic constant:

$$k_{43} = \left[A_{43}\tanh\left(\frac{T - B_{43}}{C_{43}}\right) + A_{43}\right]T \tag{45}$$

Tanh dependence of the reaction constant is very similar to modified Arrhenius equation, but it includes an ignition step—small jump on the curve of T- k_{43}, which depends on the parameter C_{43} in the formula. The selectivity coefficient of soot consumption by oxygen f_{CO} has temperature dependence given by [21,22]:

$$f_{\mathrm{CO}} = \frac{1}{1 + A_{f_{\mathrm{CO}}}\exp(E_{f_{\mathrm{CO}}}/RT)c_{\mathrm{O}_2}^{\mu_1}} \tag{46}$$

Diesel particulate matter oxidation by NO_x consists of two simultaneous reactions: direct and co-operative oxidation, both produce CO and CO_2:

$$\mathrm{C} + 2\mathrm{NO}_2 \rightarrow \mathrm{CO}_2 + 2\mathrm{NO} \tag{47}$$

$$\mathrm{C} + \mathrm{NO}_2 \rightarrow \mathrm{CO} + \mathrm{NO} \tag{48}$$

$$\mathrm{C} + \mathrm{NO}_2 + \frac{1}{2}\mathrm{O}_2 \rightarrow \mathrm{CO}_2 + \mathrm{NO} \tag{49}$$

$$\mathrm{C} + \frac{1}{2}\mathrm{O}_2 \overset{\mathrm{NO}_2}{\rightarrow} \mathrm{CO} \tag{50}$$

The above reactions describe both soot oxidation by O_2 and NO_2 separately, (43), (47) and (48), and oxidations involving simultaneously O_2 and NO_2 (49) and (50). NO_2 promotes the decomposition of the intermediate C–O complex which is formed by the O_2 chemisorption on the carbon surface. It has been shown that NO_2–O_2 mixture oxidizes soot particles faster than is the sum of oxidation rates by NO_2 and O_2 separately. In the presence of 10% of O_2 and NO_2 the reaction rate is about twice as high as that of the C–NO_2 reaction only at 300 °C [23].

Direct oxidations of carbon (47) and (48) are faster in the presence of water vapor, which has catalytic effect due to formation of trace amounts of nitric and nitrous acids (nitrous acid rapidly decomposes into nitric acid). This effect on the reaction rate of the co-operative reaction C–NO_2–O_2 was not observed [24]. On the contrary the co-operative oxidations (49) and (50) are catalyzed in the presence of platinum based catalyst, but direct oxidations are not significantly affected. Effect of Pt is in the increasing formation of key component of soot oxidation—surface complexes –C(O). Oxygen is adsorbed on the Pt and then spillovered to active carbon site to produce –C(O). –C(O) is destabilized by NO_2 to –C(O–NO_2) intermediate complex, which decomposes to CO and NO_2 or CO_2 and NO [25]. It has been reported that catalytic effect on the soot oxidation by NO_2 exhibits ruthenium based catalysts [25]. Platinum catalyst affects also other reactions such as, e.g., C–O_2, CO–O_2 or NO/NO_2, but the activity of Pt-doped catalyst depends on the contact between platinum and soot particles [26]. An exponential dependence of $k_{(47-50)}$ on temperature is considered in the model and reaction rates are determined as

$$\mathcal{R}_{47} = k_{47}\left(\frac{m_p}{\rho_p V_{\mathrm{FVM}}\varepsilon_i^0}\right)p_{\mathrm{NO}_2}^{a_{47}}(1 + b_{47}\omega_{\mathrm{H}_2\mathrm{O}}^{c_{47}}) \tag{51}$$

$$\mathcal{R}_{48} = k_{48}\left(\frac{m_p}{\rho_p V_{\mathrm{FVM}}\varepsilon_i^0}\right)p_{\mathrm{NO}_2}^{a_{48}}(1 + b_{48}\omega_{\mathrm{H}_2\mathrm{O}}^{c_{48}}) \tag{52}$$

$$\mathcal{R}_{49} = k_{49}\left(\frac{m_p}{\rho_p V_{\mathrm{FVM}}\varepsilon_i^0}\right) p_{\mathrm{NO_2}}^{a_{49}}\omega_{\mathrm{O_2}}^{d_{49}} \tag{53}$$

$$\mathcal{R}_{50} = k_{50}\left(\frac{m_p}{\rho_p V_{\mathrm{FVM}}\varepsilon_i^0}\right) p_{\mathrm{NO_2}}^{a_{50}}\omega_{\mathrm{O_2}}^{d_{50}} \tag{54}$$

The reaction C–NO_2can produce also small amounts of N_2 and thus we have included the following additional reaction [27]

$$\mathrm{C} + \mathrm{NO_2} \rightarrow \frac{1}{2}\mathrm{N_2} + \mathrm{CO_2} \tag{55}$$

with the reaction rate:

$$\mathcal{R}_{55} = k_{55}\left(\frac{m_p}{\rho_p V_{\mathrm{FVM}}\varepsilon_i^0}\right)\omega_{\mathrm{NO_2}}^{a_{55}} \tag{56}$$

Soot particulates are also combusted by NO if the temperature increases above 600 °C—the reactivity of C–NO is similar to that of C–O_2. CO_2 requires lower desorption energy than CO and the favored product for C–NO reaction is assumed to be CO_2:

$$\mathrm{C} + 2\mathrm{NO} \rightarrow \mathrm{N_2} + \mathrm{CO_2} \tag{57}$$

This reaction is much less significant in the presence of Pt catalyst—where NO is transformed by NO/NO_2 reaction (59) and the formed NO_2 oxidizes soot more rapidly than NO. Reaction (57) has been directly measured in the absence of catalyst by injecting NO into the reactor and the observed reaction rate of the C–NO reaction is approximately 7 times slower than that of C–NO_2 at 400 °C. Reaction order of C–NO reaction increases with temperature—it is near zero at 700 K and is a first-order around 1000 K [27,28]:

$$\mathcal{R}_{57} = k_{57}\left(\frac{m_p}{\rho_p V_{\mathrm{FVM}}\varepsilon_i^0}\right)\omega_{\mathrm{NO}}^{a_{57}(T)} \tag{58}$$

Kinetic parameters of k_{43} (T)– k_{57} (T) are evaluated from experimental studies on the soot combustion and DPF regeneration at different temperatures with varying inlet concentrations of oxygen, nitrogen dioxide and moisture in the presence and in the absence of platinum catalyst. Evaluated set of parameters in the absence of catalyst (e.g., Pt) is used for wall, soot and ash layer and the set of parameters evaluated for data measured with the presence of Pt is used for the washcoat layer.

4.2. Transformation NO/NO_2

If no exhaust gas recirculation (EGR) is used, then NO_2can form, e.g., 10% of the NO_x mixture. But if the exhaust gas recirculation (EGR) is used, then the NO_2 fraction in the total NO_x can be much higher. NO_2 could be generated by the following reversible reaction which takes place on catalytic sites in the wall:

$$\mathrm{NO} + \frac{1}{2}\mathrm{O_2} \leftrightarrow \mathrm{NO_2} \tag{59}$$

Reaction rate expression is in the form [29]:

$$\mathcal{R}_{59} = \frac{k_{59}}{G_1}\left(\omega_{\mathrm{NO}}\sqrt{\omega_{\mathrm{O_2}}} - \frac{\omega_{\mathrm{NO_2}}}{K_{59}^{\mathrm{eq}}}\right) \tag{60}$$

where K_{59}^{eq} is reaction equilibrium constant. Reaction rate constant depends on temperature according to Arrhenius law:

$$k_{59} = A_{59}\exp\left(\frac{-\Delta E_{a,59}}{RT}\right) \tag{61}$$

Reaction is strongly limited by the thermodynamic equilibrium. G_1 is a semiempirical modified inhibition term and it is computed from [30]:

$$G_1 = (1 + K_{a,1}\omega_{\mathrm{CO}} + K_{a,2}\omega_{\mathrm{C_3H_6}})^2(1 + K_{a,3}\omega_{\mathrm{CO}}^2\omega_{\mathrm{C_3H_6}}^2) \times (1 + K_{a,4}\omega_{\mathrm{NO}}^{0.7})T \tag{62}$$

Inhibition constants $K_{a,i}$ are defined as

$$K_{a,i} = k_{a,i}\exp\left(\frac{\Delta E_{a,i}^0}{T}\right), \quad i = 1, 4 \tag{63}$$

4.3. Hydrocarbons, CO and H_2 oxidation

The representative hydrocarbon molecule for diesel exhaust has 7 carbon atoms and the molecular ratio H/C in diesel exhaust is around 1.8 [2]. Following chemical reaction considers common representative hydrocarbon:

$$\mathrm{C}_x\mathrm{H}_y + \left(x + \frac{y}{4}\right)\mathrm{O_2} \rightarrow x\mathrm{CO_2} + \left(\frac{y}{2}\right)\mathrm{H_2O} \tag{64}$$

For representation of hydrocarbons is used propylene (C_3H_6) for purposes of this work and thus reaction (64) can be written as

$$\mathrm{C_3H_6} + \frac{9}{2}\mathrm{O_2} \rightarrow 3\mathrm{CO_2} + 3\mathrm{H_2O} \tag{65}$$

The rate expression employed in the above reaction is

$$\mathcal{R}_{65} = \frac{k_{65}\omega_{\mathrm{O_2}}\omega_{\mathrm{C_3H_6}}}{G_1} \tag{66}$$

Reactions for the oxidation of CO and H_2 are

$$\mathrm{CO} + \frac{1}{2}\mathrm{O_2} \rightarrow \mathrm{CO_2} \tag{67}$$

$$\mathrm{H_2} + \frac{1}{2}\mathrm{O_2} \rightarrow \mathrm{H_2O} \tag{68}$$

Reaction rates of both reactions are in the form adapted from Dardiotis et al. [2]:

$$\mathcal{R}_{67} = \frac{k_{67}\omega_{\mathrm{O_2}}\omega_{\mathrm{CO}}}{G_1} \tag{69}$$

$$\mathcal{R}_{68} = \frac{k_{68}\omega_{\mathrm{O_2}}\omega_{\mathrm{H_2}}}{G_1} \tag{70}$$

4.4. NO reduction

CO, H_2or hydrocarbons can be oxidized by nitrogen oxides. These reactions are slower than the combustion by O_2 under excess of oxygen and thus conversions are very low in lean diesel exhaust. However, DPF model can be also used as a part of complete exhaust system model including DOC–NSRC–DPF. Here the NSRC surface

Table 1
Simulation and evaluated parameters of the coated and uncoated silicon carbide filters with two cell densities (200 and 300 cpsi).

Parameter	Value	
Cell density (cpsi)	200	300
Wall thickness (μm)	405	340
Reactor diameter (mm)	144	144
Reactor length (mm)	154	154
Wall porosity (%)	45	40
Washcoat porosity (%)	70	70
Bulk density (kg/m^3)	1750	1380
Wall permeability (m^2)	1.2×10^{-12}	
Washcoat permeability (m^2)	1.5×10^{-13}	
Wall Forchheimer factor (m^{-1})	1.5×10^{9}	
Washcoat Forchheimer factor (m^{-1})	0	

Catalytic filter is coated by washcoat (20 g/l_{DPF}).

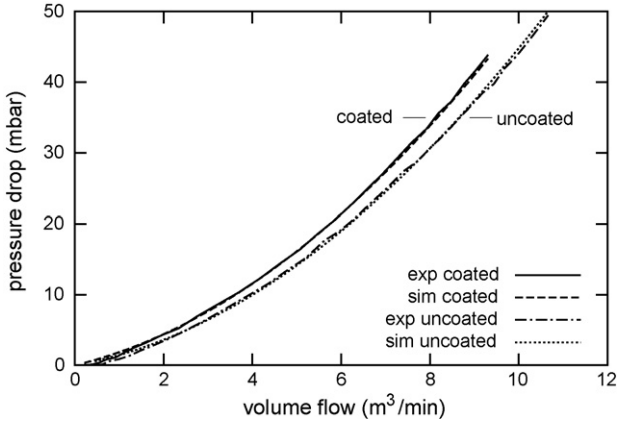

Fig. 4. Gas flow–pressure drop dependence, model validation: uncoated/coated (40 g/l_{DPF}) 300 cpsi SiC filter, 144 × 154 mm.

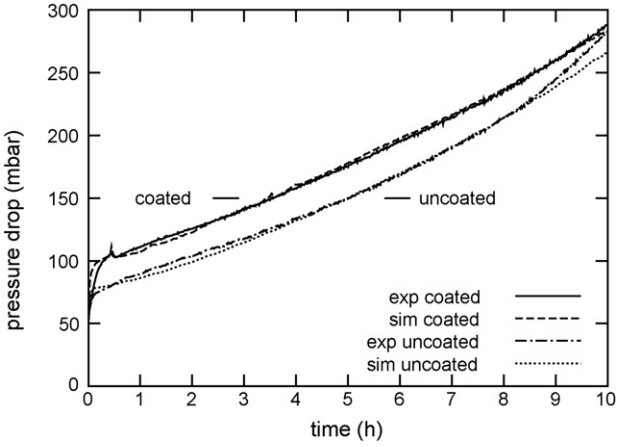

Fig. 5. Model validation for soot loading experiments: uncoated/coated (20 g/l_{DPF}) 200 cpsi SiC filter, final amount of soot 10 g/l_{DPF}.

is regenerated within short rich phases, where NO reduction is important. Hence we have assumed a single overall reaction:

$$2CO + 2NO \rightarrow 2CO_2 + N_2 \quad (71)$$

with the following reaction rate:

$$\mathcal{R}_{71} = k_{71}\omega_{CO}\omega_{NO}^{0.5} \quad (72)$$

Carbon monoxide can also react with NO_2 and produce nitrogen oxide and carbon dioxide:

$$2CO + NO_2 \rightarrow 2CO_2 + NO \quad (73)$$

This reaction occurs at lower temperatures until CO oxidation by O_2 is ignited (∼150 °C) with the reaction rate

$$\mathcal{R}_{73} = k_{73}\omega_{CO}\omega_{NO_2} \quad (74)$$

5. Results

5.1. Model validation

We have evaluated kinetic and physical parameters from different laboratory experiments and experimental data. Permeability and Forchheimer coefficient of the wall have been evaluated from

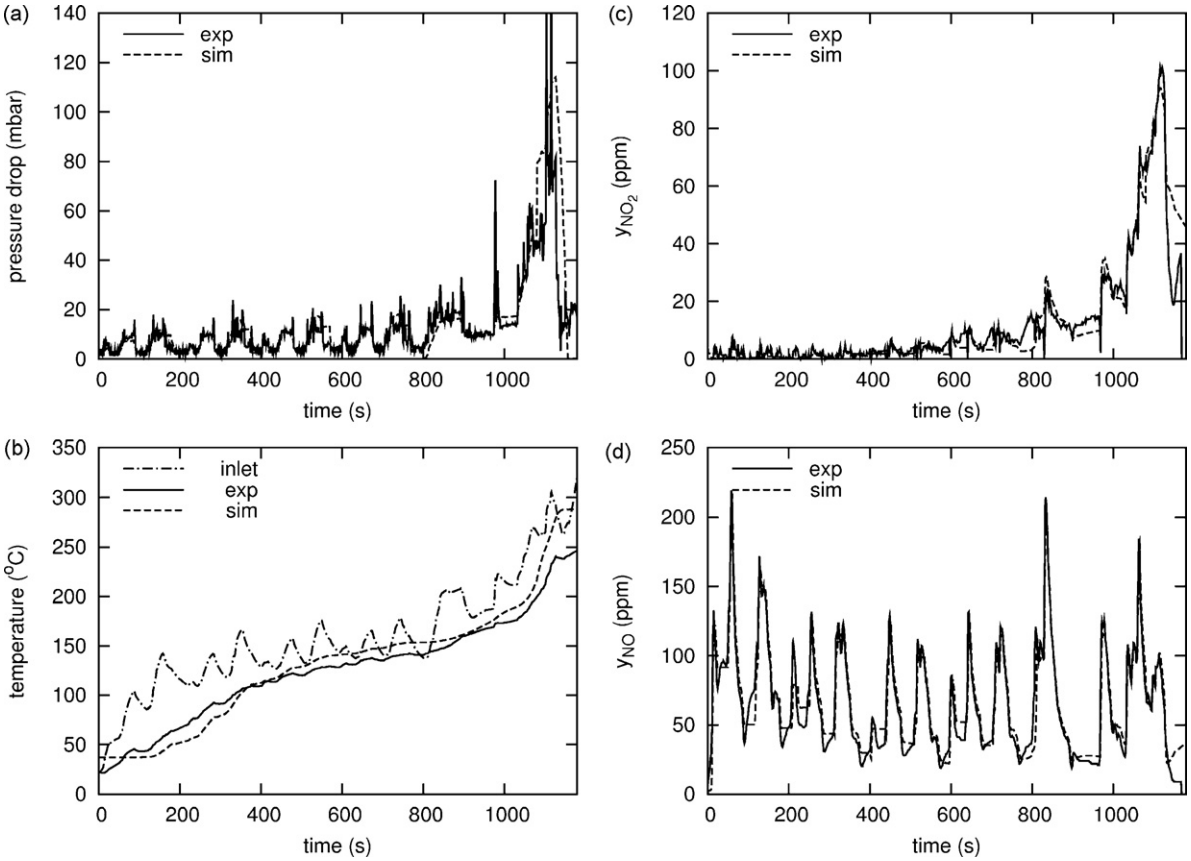

Fig. 6. Model validation on EDC (0–800 s) and EDUC (800–1180 s) experiments with vehicle: coated (20 g/l_{DPF}) 200 cpsi SiC filter. (a) Pressure drop of the filter, (b) inlet and outlet temperature of gas, (c and d) outlet concentrations of NO_2, resp. NO. Data adapted from [31].

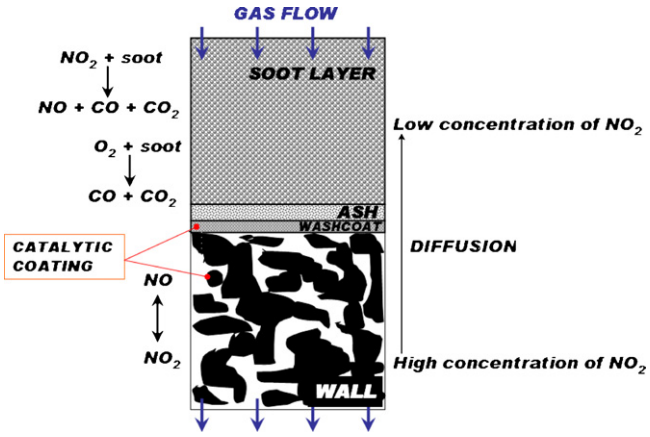

Fig. 7. Solid part section of DPF with reaction processes. Soot is oxidized in every layer and in the porous wall, produced NO is transformed back to NO_2 in washcoat layer. Pt-based coating could be also in the porous wall.

gas flow-pressure drop measurements at first. We have fitted data for two cell densities (200 and 300 cpsi) of the uncoated DPF made from silicon carbide (DPF parameters used in the simulations are listed in Table 1). The case of segmented 300 cpsi filter is depicted in Fig. 4 in comparison with the filter coated by catalyst (40 g/l_{DPF}). From the measurement of coated SiC filters we have evaluated pressure drop data of catalytical coating. With the evaluated parameters for pressure drop computation we have evaluated parameters for filter loading by soot particles—pore bridge factor, average permeability of soot layer, etc. The comparison of simulated and experimental data–time evolution of pressure drop is shown in Fig. 5. The mean soot mass flow was 0.7 mg/s and the mean space velocity 90,000 h^{-1}. The shown discrepancy between the measured and the simulated pressure drop from 9 h onwards could here follow from channel clogging. A typical Δp dependence on the loading time or loaded soot mass is in this region almost linear.

Kinetic parameters of reactions have been adapted from literature sources or evaluated from various experimental data [31]. Developed kinetic model of soot-NO_x reaction evaluated with and without platinum catalyst was validated on EDC cycle with chosen EUDC phase (cf. Fig. 6). We have used the evaluated permeability and Forchheimer coefficient of the wall and other parameters (measured by Hg porosimetry) to simulate pressure drop of the measured filter—cf. Fig. 6(a). Fig. 6(b) represents inlet temperature and simulated and experimental outlet temperature from the filter. Outlet concentrations of NO_2 and NO are depicted in Fig. 6(c) and (d). Large discrepancy in the last 50 s of the cycle follows from intensive braking from 120 kph to 0 kph. This dynamic behaviour is difficult to simulate by the stationary hydrodynamic model.

5.2. Kinetics study

We have assumed that solid parts section consists of the soot and the washcoat layers and the wall. There could be also ash layer if the diesel filter is aged (cf. Fig 7). Soot particles are trapped and oxidized in each layer. Platinum sites (or other noble group metals) are dispersed mainly in the washcoat layer or within the wall.

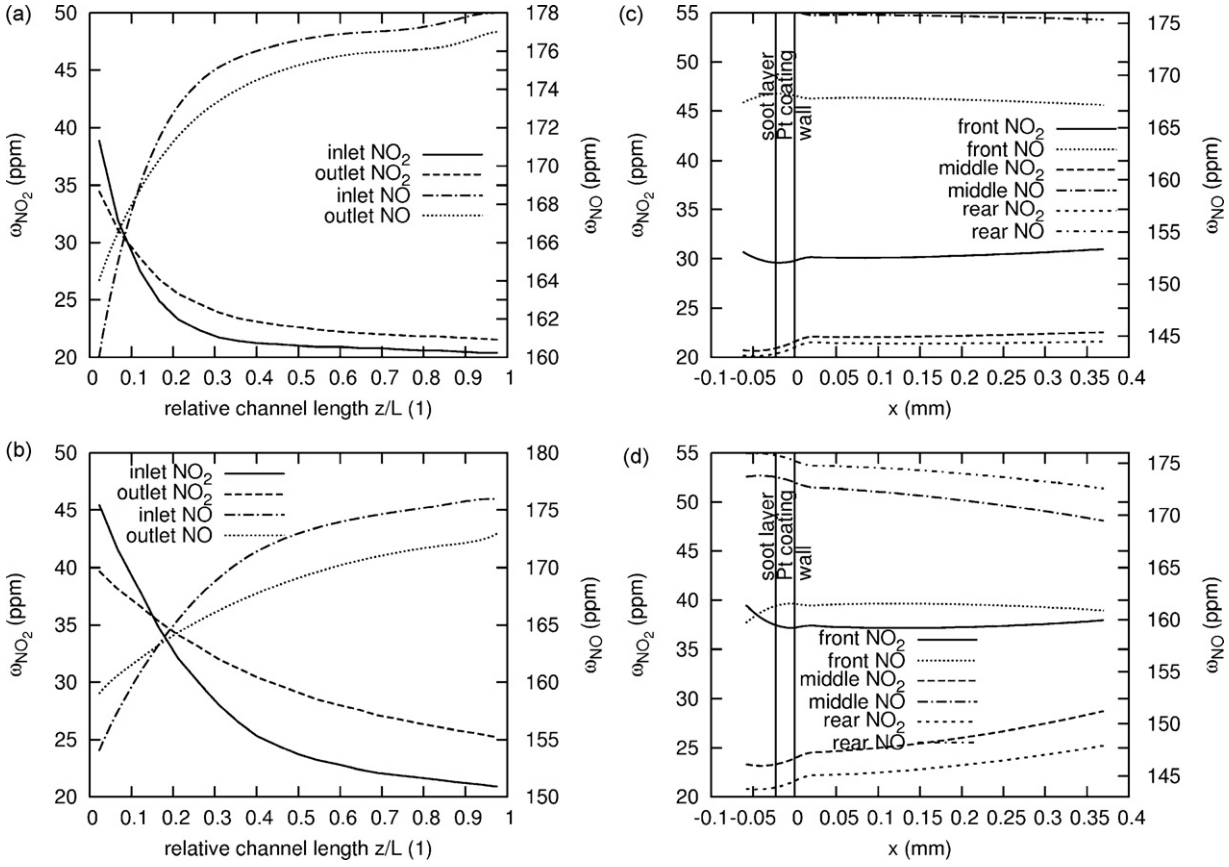

Fig. 8. Characteristic profiles of molar fraction of NO and NO_2 in the flowing gas in the inlet and the outlet channels for two different mass flows SV = 20,000 h^{-1} (a) and SV = 60,000 h^{-1} (b). Concentration of NO_2 is decreasing in the inlet channel due to mass transport of components to/from solid phase. Molar fraction of NO and NO_2 in different parts (front, middle and rear part of the channel) of the solid in the x-axis direction. NO_2 is consumed by reaction with particles in the soot layer and produced NO is regenerated in catalytic coating (20 g/l_{DPF}—23 μm thickness) $T = 300\,^{\circ}C$, $\omega^{in}_{NO} = 150$ ppm, $\omega^{in}_{NO_2} = 50$ ppm, $\omega^{in}_{O_2} = 10\%$, 300 cpsi filter, SV = 20,000 h^{-1} (c), SV = 60, 000 h^{-1} (d).

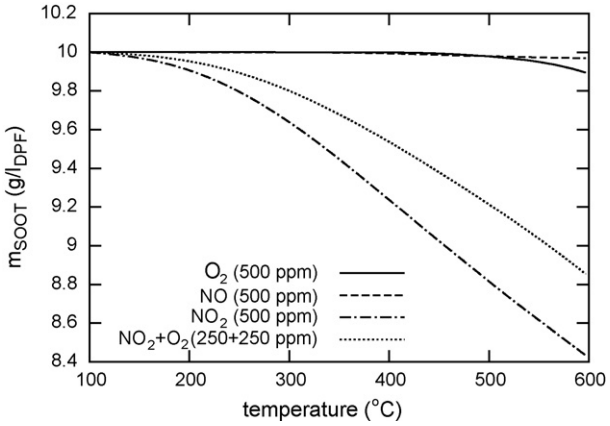

Fig. 9. Comparison of soot oxidation for four different oxidizers—NO, O_2, NO_2 and $NO_2 + O_2$ mixture, respectively. Coating 20 g/l_{DPF}, SV = 60,000 h^{-1}, 300 cpsi filter, temperature ramp 100 °C/10 min.

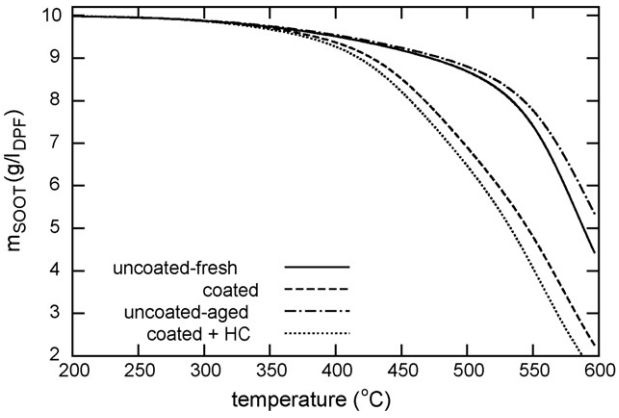

Fig. 10. Comparison of soot oxidation in four different set-ups: fresh uncoated filter, coated filter (washcoat 40 g/l_{DPF}), uncoated aged filter (ash 40 g/l_{DPF}) and coated filter (washcoat 40 g/l_{DPF}) with hydrocarbons (500 ppm) at the inlet gas. 300 cpsi filter, temperature ramp 100 °C/5 min, $\omega^{in}_{O_2} = 10\%$, $\omega^{in}_{NO_2} = 100$ ppm, $\omega^{in}_{NO} = 500$ ppm.

Catalytic coating could be either on the surface of the inlet channel wall or on the surface of both inlet and outlet walls. Soot and ash layers can contain particles of the additive catalysts (cerium oxide based catalyst added to the diesel fuel). The layer containing catalyst may affect also contacted particles in the adjoining layer. For this reason we have used the multi-layer reaction model similar to the model of soot oxidation of Konstandopoulos et al. [32]. Reaction processes are indicated in Fig. 7, soot particles are oxidized by $O_2$and NO_2in every layer. Reaction C–NO_2 produces NO, which is transformed back to NO_2 on Pt sites in the washcoat or coated pores in the wall. Then NO_2 could diffuse back to soot or ash layer. Backflow of NO_2 by diffusion depends on mass flow across solid part in the opposite direction, pore size distribution and many other parameters. As an example we have chosen temperature 300 ° C where the yield of NO_2 by NO/NO_2 transformation is close to maximum. Concentration profiles in the inlet and the outlet channels are depicted in Fig. 8 for two different space velocities—20,000 h^{-1} and 60,000 h^{-1}. Concentration profiles of NO_2 and NO differ in Fig. 8(a) and (b) because $NO_2$and NO are transferred from the flowing gas to soot layer by mass transfer described by the model of Ramanathan et al. [8]. Fig. 8(c) and (d) represents concentration profiles of $NO_2$and NO in the *x*-direction in the solid (within all layers) in the front, middle and rear parts of the channel. NO_xspecies are moved by convection flow to outlet channel and by diffusion in opposite direction according to concentration gradient. The NO_2 concentration is rising within the wall, where the concentration of soot particles is small due to higher filtration efficiency of the washcoat layer. The increase is higher in the rear part of the channel wall. NO_2 is formed on the catalyst in the washcoat and its concentration increases along the *z*-axis in the outlet channel.

Comparison of different soot reactions is shown in Fig. 9. DPF loaded by 10 g/l_{DPF} of soot matter has been heated in different flowing gases (with nitrogen as inert). Most effective burning of the soot was observed for NO_2alone; $NO_2 + O_2$ mixture is worse oxidizer than O_2, although cooperative oxidation by $NO_2 + O_2$ is enabled, the slowest oxidation rate has NO. It could be seen that 500 ppm of $NO_2 + O_2$ mixture is better as an oxidation agent than the sum of 250 ppm of O_2 and 250 ppm of NO_2, because the cooperative soot oxidation occurs. However, the cooperative oxidation is slowed in the presence of catalyst and in the absence of NO at higher temperatures. It is caused by NO_2 decomposition to NO and O_2 by the NO-NO_2 transformation.

Comparison of fresh and aged uncoated filter with the coated filter is shown in Fig. 10. The fastest soot combustion is in the case of the catalyzed filter with the addition of 500 ppm hydrocarbons at the inlet. Soot combustion following from a temperature ramp in the catalyzed filter without the effect of hydrocarbons is much faster than for the uncatalyzed filter. Difference between fresh and aged filter (e.g., with the ash layer) is quite small. The effect of Pt catalyst on C–NO_2reaction is shown in Fig. 11. This example has been computed with switched off C–O_2reaction. Soot is consumed rapidly in the presence of catalyst, as NO is easily transformed to NO_2(O_2 is present in the inlet mixture) and cooperative reaction C–NO_2–O_2 is also faster in the washcoat layer. Effect of NO_x composition in the inlet mixture is shown in Fig. 12. Coated filter with 10 g/l_{DPF} of soot has been heated in temperature ramp below the ignition temperature of C–O_2reaction. Soot content time developments are very similar for all NO/NO_2 ratios due to NO/NO_2 reaction. As a result, almost the same concentrations of NO_2 have been obtained at the outlet. Similar overall carbon oxidation rate is due to lower mass flow through solid phase (SV = 60, 000 h^{-1}, 300 cpsi) and high porosity of washcoat and wall. Then soot particles are trapped mainly in the washcoat or wall, close to NO_2 source—catalyst, and NO_2 diffusion is comparable to convection. NO_2 is thus well distributed around soot particles. Soot matter oxidation for different temperatures is depicted in Fig. 13. Soot is significantly oxidized by NO_2above 250 °C. Carbon oxidation by oxygen is ignited at temperatures higher than 450 ° C in the presence of the catalyst (or e.g., 500 ° C MoO_3/Al_2O_3[33]).

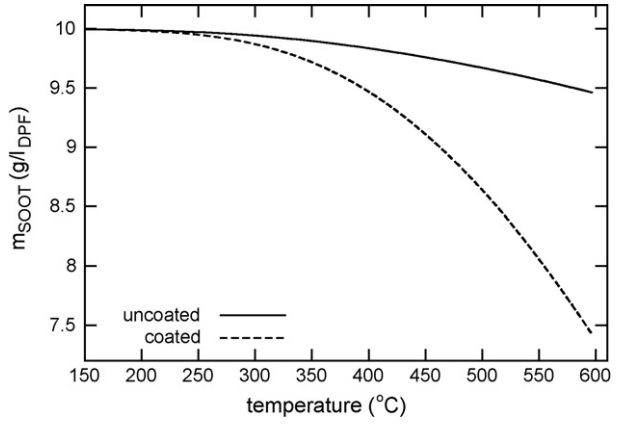

Fig. 11. Comparison of soot oxidation by C–NO_2–NO reactions (oxidation by O_2 is not assumed in this example) on uncoated and coated (40 g/l_{DPF}) filter. 300 cpsi filter, temperature ramp 100 °C/5 min, $\omega^{in}_{O_2} = 10\%$, $\omega^{in}_{NO_2} = 100$ ppm, $\omega^{in}_{NO} = 500$ ppm.

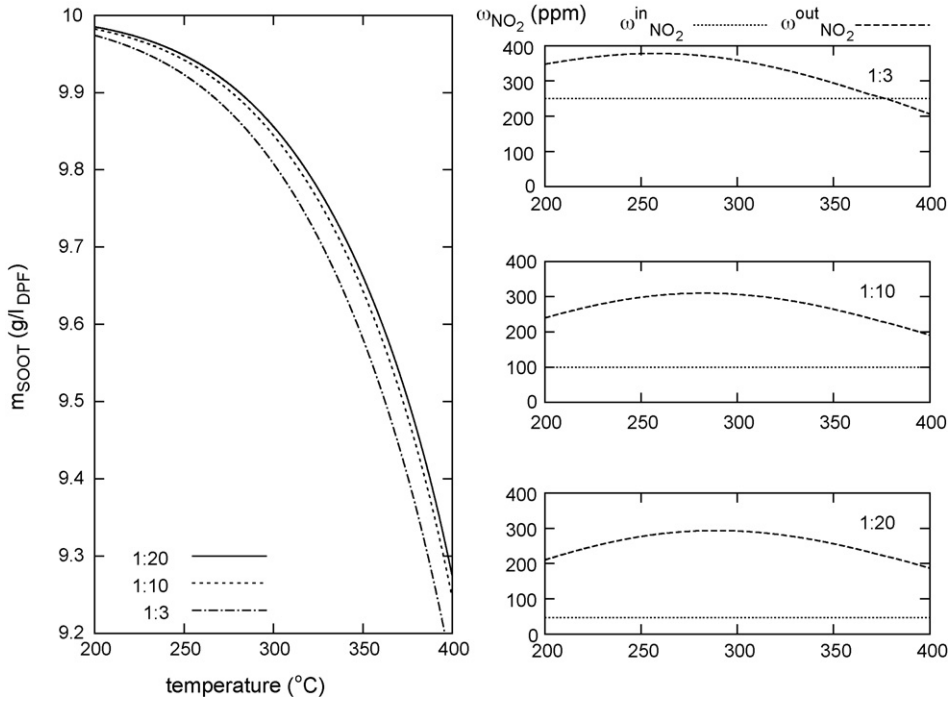

Fig. 12. Influence of ratio of NO_2/NO in the inlet gas mixture on soot combustion. Concentration of NO_x at the inlet has been 1000 ppm with NO_2/NO ratios 1:3–20 (1:10 is typical value in diesel applications). 300 cpsi filter, temperature ramp 100 °C/5 min, $\omega^{in}_{O_2} = 10\%$, $\omega^{in}_{NO_x} = 1000$ ppm, SV = 60,000 h^{-1}.

5.3. Regeneration study

Example of regeneration of diesel filter is shown in Figs. 14–16 . Fig. 14 represents time development of inlet and outlet temperature and pressure drop of DPF. Inlet temperature increased in two stages from 250 ° C to 650 ° C for the regeneration of 10 g/l_{DPF} loaded filter. Pressure drop is strongly influenced by temperature but difference between initial and final value corresponds to pressure drop due to soot loading, because initial and final temperatures are almost the same. Soot mass time dependence in whole filter and in the wall, washcoat layer and soot cake separately are depicted in Fig. 15. Two temperature steps are reflected in the soot mass curve. Soot is combusted in the washcoat much faster and the combustion starts at lower temperatures. Soot weight is increasing again at the end of the simulation due to continual trapping in the filter (soot flow =

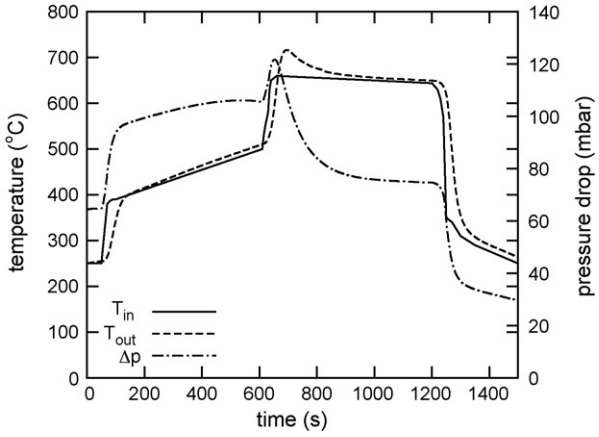

Fig. 14. Regeneration study—time development of temperature and pressure drop.

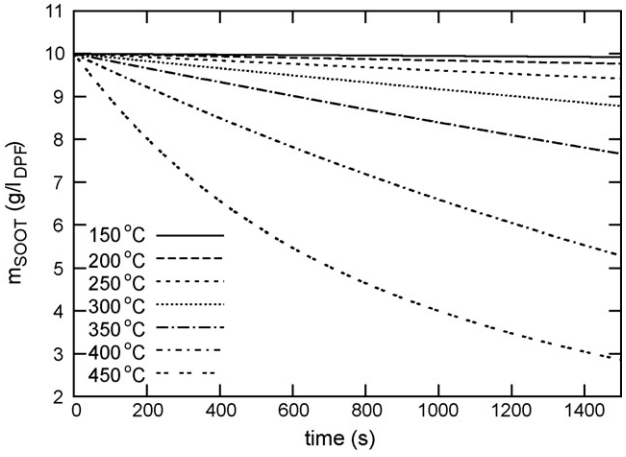

Fig. 13. Comparison of soot oxidation for different initial and inlet gas temperatures in coated (40 g/l_{DPF}) 300 cpsi filter. $\omega^{in}_{O_2} = 10\%$, $\omega^{in}_{NO_2} = 100$ ppm, $\omega^{in}_{NO} = 500$ ppm, SV = 60,000 h^{-1}.

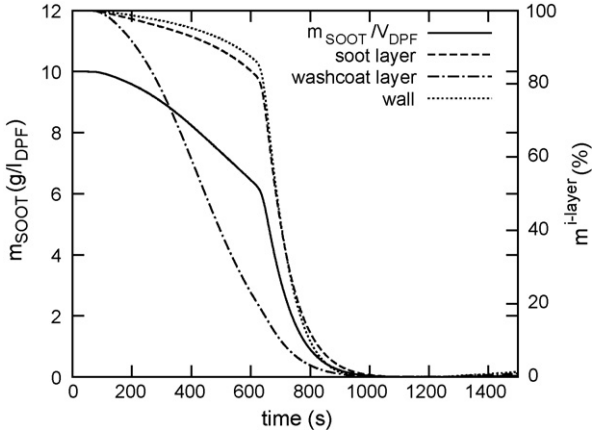

Fig. 15. Regeneration study—time development of soot weight in the filter and percentage soot weight in every layer separately.

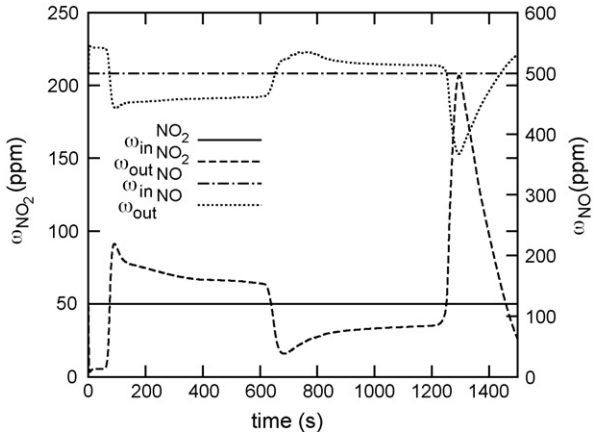

Fig. 16. Regeneration study—time development of inlet and outlet molar fraction of NO_2 and NO.

10 mg/m_{gas}^3, SV = 60, 000 h^{-1}). Inlet and resulting outlet molar fractions of $NO_2$and NO are shown in Fig. 16. $NO_2$is produced by the NO/NO_2transformation and consumed by the oxidation of soot.

6. Conclusions

The developed model of diesel particulate filter and software for its solution can be used for modelling of aged (with ash layer) or fresh filter, for skin-DPF such as cordierite filters with the cake filtration or deep-DPF such as fibres filters (deep-filtration model), coated or uncoated filters and many other combinations. Due to computational effectiveness it can be also used for kinetic parameters evaluation from measured data and for simulations of design and regeneration strategies. Software could be also implemented as a part of package for simulations of whole exhaust system including models of DOC, NSRC and DPF [34].

Nomenclature

A	area (m^2)
A_{DPF}	DPF frontal area (m^2)
A, B, C, D	reaction rate coefficients
c	gas concentration ($mol\,m^{-3}$)
C_p	specific heat capacity of wall ($J\,kg^{-1}\,K^{-1}$)
d	channel diameter (m)
d_c	unit collector diameter (m)
d_p	mean pore size (m)
D	diffusion coefficient ($m^2\,s^{-1}$)
D_{DPF}	DPF diameter (m)
E_{DP}	soot particulate source (s^{-1})
exp	experimental
f_{CO}	selectivity coefficient (1)
G	inhibition term
h_z, h_x	discretization step (m)
H	enthalpy source ($J\,s^{-1}\,m^{-1}$)
J	number of components (1)
K_a	inhibition constant
k	reaction rate constant permeability (m^2)
k_b	Boltzmann constant ($1.3806503 \times 10^{-23}\,m^2\,kg\,s^{-2}\,K^{-1}$)
k_c	mass transfer coefficient ($m\,s^{-1}$)
k_h	heat transfer coefficient ($J\,s^{-1}\,m^{-2}\,K^{-1}$)
Ku	Kuwabara's hydrodynamic factor (1)
L	channel length (m)
$\dot{m}$	mass flow ($kg\,s^{-1}$)
M	molar weight ($kg\,mol^{-1}$)
m	mass (kg)
N_{UN}	number of unit collectors (1)
N_{chan}	number of inlet channels (1)
N_x	number of discretization volumes in axial direction
n_ξ	reaction order
OFA	open frontal area (m^2)
p	pressure (Pa)
P	perimeter (m)
Pe	Péclet number (1)
$\mathcal{R}$	reaction rate ($mol\,s^{-1}\,m^{-3}$)
R	universal gas constant ($8.314\,J\,mol^{-1}\,K^{-1}$)
sim	simulated
SCF	Stokes–Cunningham slip correction factor (1)
t	time (s)
T	temperature (K)
S	heat source term ($J\,s^{-1}\,m^{-1}$)
v	linear velocity ($m\,s^{-1}$)
V	volume (m^3)
w	particulate layer thickness (m)
w_s, w_{al}, w_{wl}	wall, ash layer and washcoat layer thickness (m)
x	radial coordinate (m)
y	mass fraction of component (1)
z	axial coordinate (m)

Greek letters

α	friction coefficient (1)
α_f	volume fraction of spheres/fibers (1)
β	Forchheimer factor (m^{-1})
ΔE_a	activation energy ($J\,mol^{-1}$)
ΔH^r	standard reaction enthalpy ($J\,mol^{-1}$)
ϵ	porosity (1)
η	efficiency (1)
ϕ	mass flux ($kg\,m^{-2}\,s^{-1}$)
λ	thermal conductivity ($W\,m^{-1}\,K^{-1}$)
μ	viscosity (Pa s)
μ_1	selectivity parameter (1)
ρ	density ($kg\,m^{-3}$)
τ	tortuosity (1)
ω	molar fraction of component (1)
ζ	pressure loss correlation (1)

Subscripts and superscripts

1	inlet channel
2	outlet channel
atm	atmospheric
eff	effective
conv	convection
D	diffusion
eq	equilibrium
FVM	finite volume method
g	gas
in	inlet
ini	initial
j	component index
k	reaction index
out	outlet
p	particulate, pore
R	interception
react	reaction
S	solid
transf	heat transfer
vol	volume

Acknowledgements

The work was supported by the Czech Grant Agency (grant No. 104/08/H055) and the Czech Ministry of Education (project MSM 6046137306).

References

[1] http://www.dieselnet.com(2008).
[2] Ch.K. Dardiotis, O.A. Haralampous, G.C. Koltsakis, Catalytic oxidation in wall-flow reactors with zoned coating, Chem. Eng. Sci. 63 (4) (2008) 1142–1153.
[3] Y. Yong, Simulating the soot loading in wall-flow DPF using a three-dimensional macroscopic model, SAE Technical Paper, 2006-01-0264, 2006.
[4] O.A. Haralampous, G.C. Koltsakis, Oxygen diffusion modeling in diesel particulate filter regeneration, AIChE J. 50 (2004) 2008–2019.
[5] A.S. Shende, J.H. Johnson, S.L. Yang, S.T. Bagley, A.M. Thalagavara, The filtration and particulate matter oxidation characteristics of a catalyzed wall-flow diesel particulate filter: experimental and 1-D, 2-layer model results, SAE Technical Paper, 2005-01-0949, 2005.
[6] E.J. Bissett, Mathematical model of the thermal regeneration of a wall-flow monolith diesel particulate filter, Chem. Eng. Sci. 39 (1984) 1233–1244.
[7] O.A. Haralampous, G.C. Koltsakis, Intra-layer temperature gradients during regeneration of diesel particulate filter, Chem. Eng. Sci. 57 (2002) 2345–2355.
[8] K. Ramanathan, V. Balakotaiah, D.H. West, Light-off criterion and transient analysis of catalytic monoliths, Chem. Eng. Sci. 58 (2003) 1381–1405.
[9] A.G. Konstandopoulos, M. Kostoglou, E. Skaperdas, E. Kladopoulou, D. Zarvalis, E. Papaioannou, Fundamental studies of diesel particulate filters: transient loading, regeneration and aging, SAE Technical Paper, 2000-01-1016, 2000.
[10] I.P. Kandylas, O.A. Haralampous, G.C. Koltsakis, Diesel soot oxidation with NO_2: engine experiments and simulations, Ind. Eng. Chem. Res. 41 (2002) 5372–5384.
[11] G. Gaiser, P. Mucha, Prediction of pressure drop in diesel particulate filters considering ash deposit and partial regenerations, SAE Technical Paper, 2004-01-0158, 2004.
[12] R.H. Idelchik, Flow Resistance: A Design Guide for Engineers, Hemisphere Publication, 1989.
[13] O.A. Haralampous, G.C. Koltsakis, Back-diffusion modeling of NO_2 in catalyzed diesel particulate filters, Ind. Eng. Chem. Res. 43 (2004) 875–883.
[14] B.E. Poling, J.M. Prausnitz, J.P. O'Connell, The Properties of Gases and Liquids, Mc Graw-Hill, New York, 2000.
[15] G.C. Koltsakis, A. Konstantinou, O.A. Haralampous, Z.C. Samaras, Measurement and intra-layer modeling of soot density and permeability in wall-flow filters, SAE Technical Paper, 2006-01-0261, 2006.
[16] A.T. Padilla, Development of models to study the emissions, flow, and kinetic characteristics from diesel oxidation catalysts and particulate filters, Ph.D. Thesis, Michigan Technological University, 2005.
[17] H. Mohammed, A.P. Triana, S.L. Yang, J.H. Johnson, An advanced 1D 2-layer catalyzed diesel particulate filter model to simulate: filtration by the wall and particulate cake, oxidation in the wall and particulate cake by NO_2 and O_2, and regeneration by heat addition, SAE Technical Paper, 2006-01-0467, 2006.
[18] A.G. Konstandopoulos, J.H. Johnson, Wall-flow diesel particulate filters—their pressure drop and collection efficiency, SAE Technical Paper, 890405, 1989.
[19] G. Neri, L. Bonaccorsi, A. Donato, C. Milone, M.G. Musolino, A.M. Visco, Catalytic combustion of diesel soot over metal oxide catalysts, Appl. Catal. B: Environ. 11 (2) (1997) 217–231.
[20] A. Bueno-López, K. Krishna, B. van der Linden, G. Mul, J.A. Moulijn, M. Makkee, On the mechanism of model diesel soot-O_2 reaction catalysed by Pt-containing La^{3+}-doped CeO_2: a TAP study with isotopic O_2, Catal. Today 121 (3–4) (2007) 237–245.
[21] J.P.A. Neeft, T.X. Nijhuis, E. Smakman, M. Makkee, J.A. Moulijn, Kinetics of the oxidation of diesel soot, Fuel 76 (1997) 1129–1136.
[22] A.G. Konstandopoulos, M. Kostoglou, Reciprocating flow regeneration of soot filters, Combust. Flame 121 (2000) 488–500.
[23] F. Jacquot, V. Logie, J.-F. Brilhac, P. Gilot, Kinetics of the oxidation of carbon black by NO_2: influence of the presence of water and oxygen, Carbon 40 (2002) 335–343.
[24] M. Jeguirim, V. Tschamber, J.-F. Brilhac, P. Ehrburger, Oxidation mechanism of carbon black by NO_2: effect of water vapour, Fuel 84 (2005) 1949–1956.
[25] V. Tschamber, M. Jeguirim, K. Villani, J. Martens, P. Ehrburger, Comparison of the activity of Ru and Pt catalysts for the oxidation of carbon by NO_2, Appl. Catal. B: Environ. 72 (2007) 299–303.
[26] K. Hinot, H. Burtscher, A.P. Weber, G. Kasper, The effect of the contact between platinum and soot particles on the catalytic oxidation of soot deposits on a diesel particle filter, Appl. Catal. B: Environ. 71 (2007) 271–278.
[27] B.R. Stanmore, V. Tschamber, J.-F. Brilhac, Oxidation of carbon by NO_x, with particular reference to NO_2 and N_2O, Fuel 87 (2008) 131–146.
[28] E.G. Garijo, A.D. Jensen, P. Glarborg, Kinetic study of NO reduction over biomass char under dynamic conditions, Energy Fuels 17 (2003) 1429–1436.
[29] P. Kočí, Catalytic monolith reactors with surface deposition of gas components—applications in automobile exhaust gas conversion, PhD. Thesis, Institute of Chemical Technology, Prague, 2005.
[30] S.E. Voltz, C.R. Morgan, D. Liederman, S.M. Jacob, Kinetic study of carbon monoxide and propylene oxidation on platinum catalysts, Ind. Eng. Chem. Prod. Res. Develop. 12 (1973) 294–301.
[31] T. Maunula, P. Matilainen, M. Louhelainen, P. Juvonen, T. Kinnunen, Catalyzed particulate filters for mobile diesel applications, SAE Technical Paper, 2007-01-0041, 2007.
[32] A.G. Konstandopoulos, M. Kostoglou, S. Lorentzou, C. Pagkoura, E. Papaioannou, K. Ohno, K. Ogyu, T. Oya, Soot oxidation kinetics in diesel particulate filters, SAE Technical Paper, 2007-01-1129, 2007.
[33] F.S. Toniolo, E. Barbosa-Coutinho, M. Schwaab, I.C.L. Leocadio, R.S. Aderne, M. Schmal, J.C. Pinto, Kinetics of the catalytic combustion of diesel soot with MoO_3/Al_2O_3 catalyst from thermogravimetric analyses, Appl. Catal. A: Gen. 342 (2008) 87–92.
[34] http://www.vscht.cz/monolith, 2008.